Liquid Crystals
Publication details, including instructions for authors and subscription information:
http://www.informaworld.com/smpp/title~content=t713926090

Anisotropic phases of six positional isomers of n-butyl stearate and factors influencing their mesomorphism

Jon E. Baldvins; Richard G. Weiss

Online publication date: 06 August 2010

To cite this Article Baldvins, Jon E. and Weiss, Richard G.(1999) 'Anisotropic phases of six positional isomers of n-butyl stearate and factors influencing their mesomorphism', Liquid Crystals, 26: 6, 897 — 912
To link to this Article: DOI: 10.1080/026782999204598
URL: http://dx.doi.org/10.1080/026782999204598

LIQUID CRYSTALS, 1999, VOL. 26, NO. 6, 897–912

Anisotropic phases of six positional isomers of *n*-butyl stearate and factors influencing their mesomorphism

JON E. BALDVINS and RICHARD G. WEISS*

Department of Chemistry, Georgetown University, Washington, DC 20057-1227, USA

(*Received 16 May 1997; accepted 13 January 1998*)

Six positional isomers of the known mesogen, *n*-butyl stearate (**BS**), have been synthesized and their neat anisotropic phases have been investigated by optical microscopy, differential scanning calorimetry, and powder X-ray diffractometry. Pentyl heptadecanoate (**1a**), hexadecyl hexanoate (**1d**), heptadecyl pentanoate (**1e**), and octadecyl butanoate (**1f**) form enantiotropic mesophases, some of which are hexatic B or crystal B. Hexyl hexadecanoate (**1b**) forms a monotropic mesophase, and decyl dodecanoate (**1c**) is not mesomorphic. Mixtures of **BS** and **1f** are miscible in all phases and at all compositions. The factors responsible for the variations in phase behaviour among the set of isomers is discussed and compared with the properties of the analogous solid phases of *n*-heneicosane ($C_{21}H_{44}$).

1. Introduction

The term *mesophase* encompasses *plastic crystals* (in which molecules are positionally ordered, but orientationally disordered [1, 2]), *condis crystals* (or conformationally disordered solids possessing significant positional and orientational order [3]), and *liquid crystals* (in which molecules exhibit orientational order and varying degrees of positional order [4–8]). The features distinguishing thermotropic liquid crystals and condis crystals have been discussed in detail by Wunderlich and co-workers [9]. The enthalpic and entropic contributions to the overall free energy that determine the nature of a phase can be delicately balanced; it is possible to transform some condis crystals into liquid crystals (and *vice versa*) by seemingly innocuous changes in composition or structure [10]. For example, we have shown that mixtures of molecules, none of which alone is liquid crystalline, can provide thermotropic smectic phases [11].

Since *n*-alkanes, none of which are liquid crystalline [12–14], can form a variety of condis phases as mixtures, only a small increase in free energy (N.B., entropy), introduced *inter*molecularly, is required to alter the nature of the packing and, perhaps, induce liquid crystallinity [10]. An example is the polymorphism induced in *n*-heneicosane (**C21**; $C_{21}H_{44}$) upon addition of homologous *n*-alkanes [15]. Alternatively, entropy can be increased *intra*molecularly (and additional mesomorphism *may* be induced) by placing an appropriate functional group, like carboxy, along the backbone of **C21** [10], leading to various isomers of $C_{22}H_{44}O_2$.

$H(CH_2)_{21}H$ **C21**	$H(CH_2)_mO(CO)(CH_2)_nH$	
	m	*n*
BS	4	17
1a	5	16
1b	6	15
1c	10	11
1d	16	5
1e	17	4
1f	18	3

Depending upon the orientation of 'insertion' of the carboxy group at C_4–C_5 of **C21**, either heptadecyl† pentanoate (**1e**; a molecule whose mesophase properties are unknown) or *n*-butyl stearate (**BS**; a molecule whose anisotropic condensed (α) phases have been investigated extensively for more than 40 years [13]) is obtained. Since individual molecules of **BS** are relatively unreactive and contain no chromophores absorbing above *c.* 240 nm, we [16–23] and others [24–26] have employed the α phases of **BS** to investigate the influence of anisotropic environments on the photochemical and thermal reactivities of a variety of guest molecules [27, 28]. In that regard, it would be useful to employ *positional* isomers of **BS** as anisotropic media [29]. Here, we characterize the anisotropic phases of **1a**–**f**—six isomeric esters of **BS** in which the carboxy group is moved along the polymethylene chain—by optical microscopy (OM), differential scanning calorimetry (DSC), and powder

*Author for correspondence; e-mail: weissr@gusun.georgetown.edu

†All alkyl radicals are understood to be in the *n*-form.

Journal of Liquid Crystals ISSN 0267-8292 print/ISSN 1366-5855 online
http://www.tandf.co.uk/JNLS/lct.htm
http://www.taylorandfrancis.com/JNLS/lct.htm

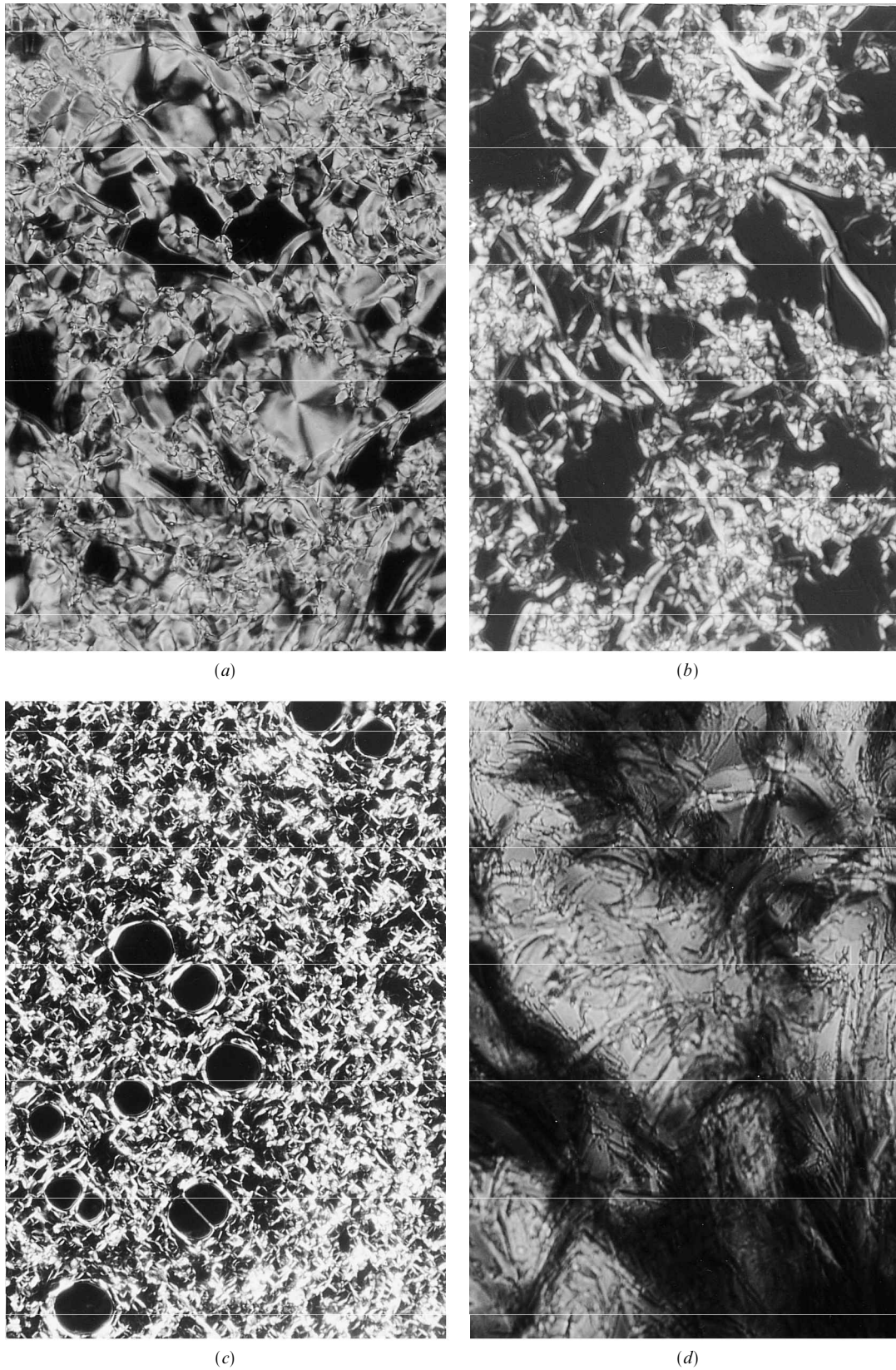

(*a*) (*b*)

(*c*) (*d*)

Figure 1. Optical micrographs (between crossed polarizers) of **BS** and **1a–f**. Magnification is *c*. X250 for (**a**, **b**, **d**, **e**) and *c*. X125 for (**c**, **f**). (*a*) α_1 phase of **BS** at 17.7°C; (*b*) smectic phase of **1f** at 17.8°C; (*c*) smectic phase of **1a** at 15.5°C; (*d*) solid phase of **1c** at 9.8°C; (*e*) mesophase of **1d** at 9.2°C; (*f*) smectic phase of **1e** at 14.0°C.

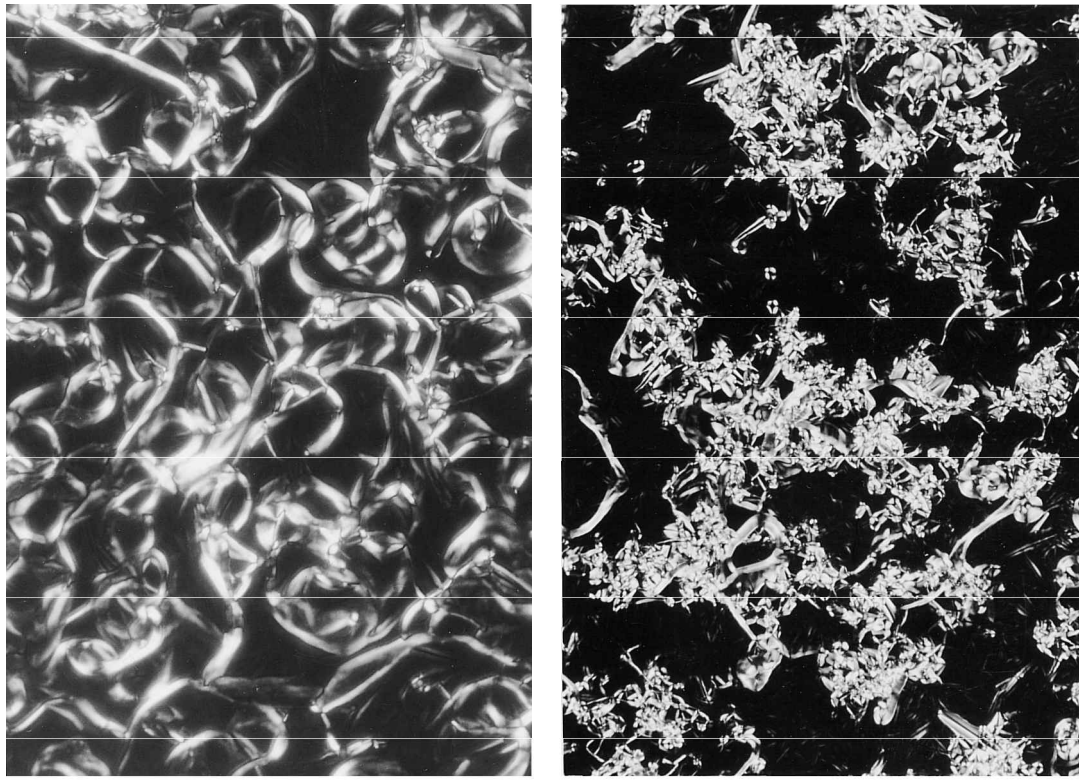

(*e*) (*f*)

Figure 1. (*continued*).

X-ray diffraction (XRD). Possible reasons for differences in the types of phases formed by the isomers are discussed in the context of structural factors and electronic interactions.

2. Results

2.1. *Prior characterization of the α phases of* ***BS***

The three anisotropic condensed (α) phases of **BS** have been investigated extensively using polarized optical microscopy (POM), powder XRD, DSC, NMR, IR, and dielectric absorption techniques [30–33]. In all, **BS** molecules are, on average, in extended conformations and arranged in layers with their long axes normal to the layer planes. There are marked similarities between the molecular packing arrangements and conformational mobilities of the lower temperature solid phases of **BS** and Phases I and II of **C21**.

Between 15 and 26°C (the clearing temperature, T_{iso}), the α_1 phase has the structural and rheological characteristics of a smectic B (SmB) [34, 35]. Molecules are arranged hexagonally in layers, and rotation occurs about the long molecular axes [34]. There are three-dimensional long range correlations [36, 37], and shear can occur within and between molecular layers. Unfortunately, the data do not distinguish between crystalline B and hexatic B phase types [35], and our additional measurements do not resolve the ambiguity. For the sake of further discussion, only the smectic B designation will be made.

In the solid-like α_2 phase (11 to 15°C), rotations about the long molecular axis are restricted and packing becomes orthorhombic [30–34]. Another crystalline phase (α_3) is formed below 11°C. It is similar in many respects to the α_2 phase, but less well-defined and with frozen rotational motions.

When **BS** is annealed for very long periods or crystallized from solvent, a solid phase whose layer thickness is 26.6 Å, instead of the thickness of the α phases (31.7 Å), is obtained [33].

2.2. *Polarized optical microscopy*

Unless noted otherwise, optical micrographs were recorded (between crossed polarizers) on thin samples that were cooled to the temperatures indicated from the isotropic phase. Gentle pressure on samples of **BS**, **1a**, **1d**, **1e**, and **1f** at temperatures slightly below T_{iso} led to some pattern distortion and flow.

The micrograph of the α_1 phase of **BS** consists of homeotropic plates with smooth edges, figure 1 (*a*). In the α_2 phase, some birefringent needle-like structures appear and fill the field in the lowest temperature α_3 phase.

Optical textures of the phases of **1f** resemble those of **BS** (N.B., figure 1 (*b*) for the α_1 phase of **1f**), but the transitions to the α_2 and α_3 phases are difficult to detect. A phase diagram for mixtures of **BS** and **1f** from optically detected transitions is virtually the same as one based upon calorimetric data (see below); measurements were reproducible within ± 0.5°C. All mixtures exhibited thermally reversible formation of the three α phases, and there was no indication of additional phases or phase separation. **BS** and **1f** are completely miscible in all proportions and at all temperatures investigated; the highest temperature anisotropic phase of **1f** must be SmB, also.

Optical micrographs of **1a** slightly below T_{iso} were consistent with a mesophase, figure 1 (*c*), while **1b** appeared to pass directly from its isotropic phase to a solid whose optical pattern resembles that of solid **1a**. The fan-like texture of solid **1c**, figure 1 (*d*), is unlike that of any of the other esters. The optical textures of the phases of **1d**, figure 1 (*e*), and **1e**, figure 1 (*f*), slightly below T_{iso} are similar to the SmB patterns of **BS** (and **1f**), but have larger domains. Slow cooling of **1d** to its lower temperature anisotropic phase produces a fan-like texture. The textures of the meso and solid phases of **1e** include some birefringent disks with Maltese crosses.

2.3. *Differential scanning calorimetry*

The initial DSC thermograms of the solvent-crystallized esters (figure 2) and **BS**/**1f** mixtures (figure 3) at 2° min^{-1} heating and cooling rates are reproduced for the second heating/cooling cycle. To ensure complete melting and mixing, samples were annealed at several degrees above T_{iso} for several minutes before cooling.

Tables 1 and 2 summarize the onset of the transition temperatures, heats of individual transitions during heating and cooling, and the sums of the transition enthalpies. Where comparisons are possible, the transition temperatures measured by POM and DSC are reasonably consistent. Transition temperatures from the **BS** thermogram match the published data [31, 33]. The relative enthalpic contents of related transitions (ΔH) and the total enthalpy changes of **BS** and **1f** are remarkably similar. They should be compared with the ΔH of the phase I–phase II (52.1 J g^{-1}) and phase II–isotropic (160.7 J g^{-1}) transitions of **C21** [12].

Entropies of transition (ΔS) in table 3 have been calculated from equation (1) for the thermodynamically reversible transitions using the values of ΔH from heating curves (ΔH_h) and the average of the onset transition temperatures from heating and cooling ($\langle T \rangle$). Since the solid–isotropic transition of **1b** is not completely reversible, the calculated value of ΔS provides only a *relative magnitude* for comparison with the other clearing transitions.

$$\Delta S = \Delta H_h / \langle T \rangle . \quad (1)$$

Table 1. Phase transition temperatures (onset) and enthalpies of transition for **BS** and **1a–f** observed by DSC on sample heating.

Compound	Transition temp./°C	Enthalpy/J g^{-1}
BS	11.1	7.5
	14.9	4.8
	26.1	107
1a	12.2	36.9
	19.6	84.2
1b	14.4	165
1c	20.0	187
1d	11.9	43.5
	13.1	81.1
1e	8.5	32.3
	12.9	2.3
	20.3	106
1f	3.3	10.5
	11.3	4.0
	23.9	104

Table 2. Transition temperatures (onset) and enthalpies of transition for **BS** and **1a–f** from DSC on sample cooling.

Compound	Transition temp./°C	Enthalpy/J g^{-1}
BS	10.6	– 5.9
	13.8	– 6.1
	25.7	– 109
1a	4.0	– 23.1
	8.5	– 1.4
	10.5	– 4.6
	20.3	– 100
1b	0.7	– 20.2
	7.1	– 20.5
	14.7	– 102
1c	19.4	– 188
1d	7.6	– 36.6
	9.1	– 7.0
	12.8	– 79.9
1e	0.9	– 21.3
	9.0	– 10.9
	12.9	– 3.8
	19.8	– 108
1f	4.2	– 9.7
	11.9	– 4.0
	24.1	– 106

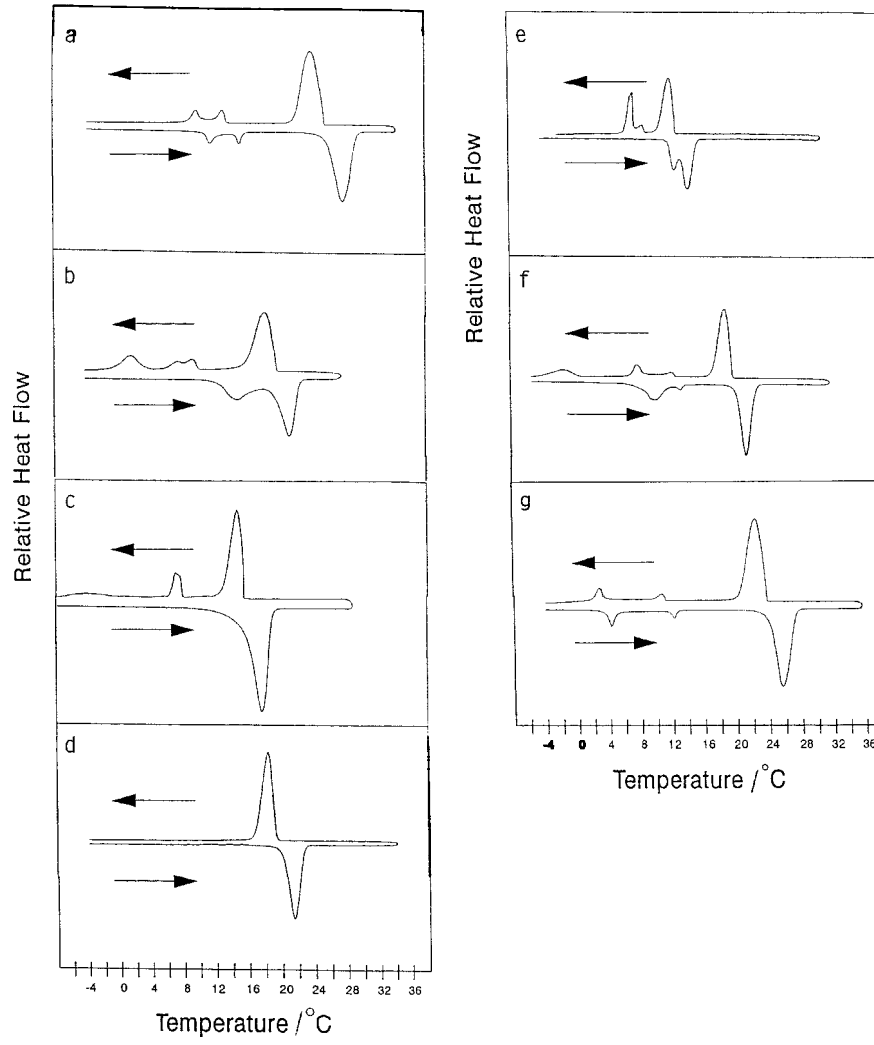

Figure 2. Thermograms of (*a*) **BS**, (*b*) **1a**, (*c*) **1b**, (*d*), **1c**, (*e*) **1d**, (*f*) **1e** and (*g*) **1f**. Sample heating precedes sample cooling.

The magnitudes of enthalpic and entropic changes can usually be related to the extent of molecular reorganization during a phase change [38–40]. The largest changes for **BS** and its positional isomers occur at the clearing transition. The transition entropies of the clearing transitions are about one order of magnitude larger than those of the lower temperature solid–solid or solid–smectic transitions. In addition, the ΔS values associated with the solid–isotropic transitions are more than 50% larger than those from the smectic–isotropic transitions. The ΔS between the solid phases of **C21** (0.17 J g^{-1} K^{-1}, as calculated from published data [12]) is about one order of magnitude larger than for the analogous transitions of **BS** and the **1** isomers; the magnitude of the entropy change of the solid–isotropic transition of **C21** (0.51 J g^{-1} K^{-1} [12]) is between the smectic–isotropic and solid–isotropic values of the esters.

Figure 4 shows the onset transition temperatures (heating) as a function of mol % of **1f** in mixtures with **BS**. Similar results were found upon cooling. The lack of additional peaks in **BS**/**1f** thermograms (figure 3) and the very small depression of the transition temperatures confirm the conclusion from POM that the two esters are miscible in all compositions and at all temperatures.

2.4. *Powder X-ray diffraction measurements*

XRD patterns were recorded at temperatures within the different phases. The low angle diffraction peaks are related to lamellar repeat distances, d, which are obtained from Bragg's law [41]. When possible, d-spacings have been calculated from higher order (0 0 1) or (0 0 0 1) reflections. The d values of the α phases of **BS** are known to be equal to the extended molecular length [30].

For some esters, intermolecular distances and intralayer packing arrangements can be deduced from the appearance and position of the high angle peaks ($2\theta \approx 20$–$30°$). We assume that a single (1 0 0 0) symmetrical peak is related to the intermolecular distance (D) for an array of hexagonally-packed molecules

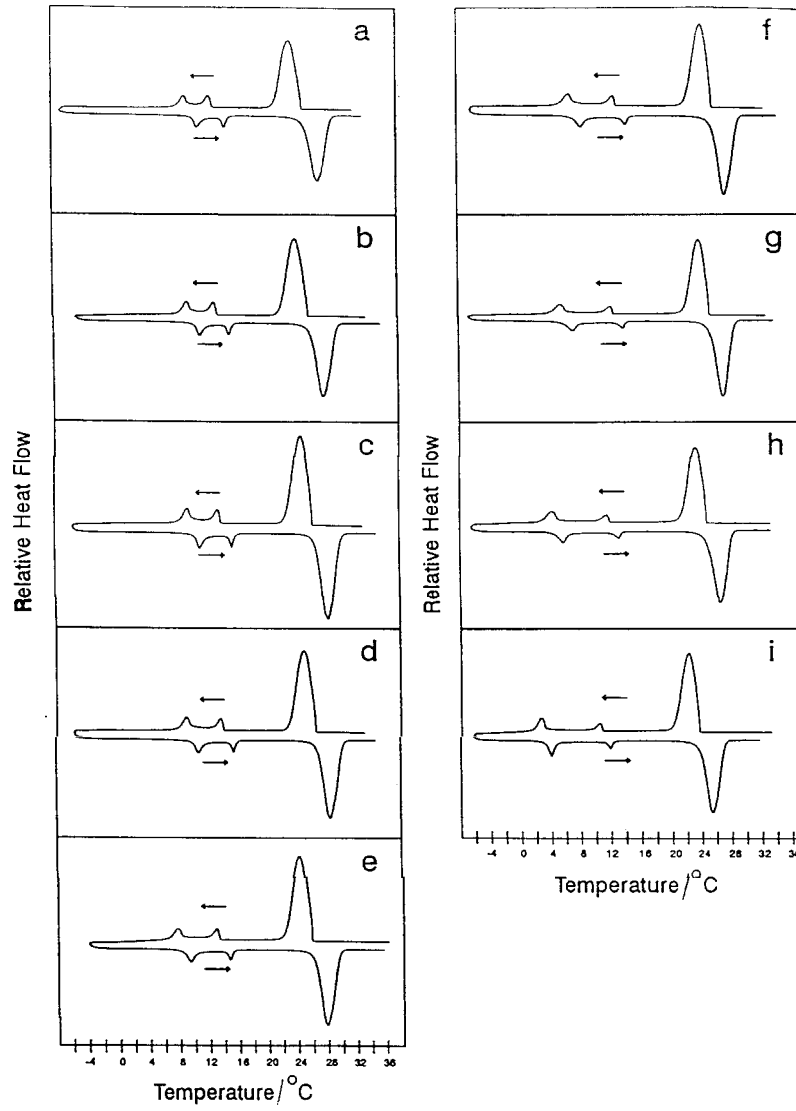

Figure 3. Heating and cooling thermograms of a series of **BS/1f** mixtures. The weight % of **1f** are (*a*) 0, (*b*) 12.8, (*c*) 25.5, (*d*) 37.2, (*e*) 50.0, (*f*) 61.6, (*g*) 75.0, (*h*) 87.6, and (*i*) 100.

[31]. Two and/or three peaks at high angle indicate orthorhombic packing as a result of intermolecular interactions, damping of rotational motions about the molecular long axes, and a concomitant lowering of the packing symmetry [31, 41].

Azimuthal widths of high angle reflections are useful in determining if a sample has preferred orientations [42]. Rotations of our samples by 90° resulted in changes of peak intensity. The largest increases, about 220%, for the (0 0 1) peak and 70% for the (1 0 0) peak, were found for the 1/1 **BS/1f** mixture at 18°C. A correlation between changes in the (0 0 1) and (1 0 0) peak intensities was not apparent upon rotation of other samples. None was expected, due to the orthogonality of the two lattice parameters responsible for these reflections. Furthermore, since the samples had concave surfaces, the intensity data are intrinsically angle-dependent and of limited value. In general, repeated scans of a sample at one temperature were reproducible to better than ± 0.5 Å for d from the (least precise) lowest angle diffractions.

X-ray diffractograms of **C21** at 26 and 38°C (warmed sample) (figure 5) provide evidence for long range packing order. In Phase I (*a*), at least nine orders of the low angle (0 0 1) d-spacings are present; in the 'rotator' Phase II (*b*), six orders of the low angle (0 0 0 1) d-spacings can be detected. The two peaks at higher angle in the Phase I diffractogram are consistent with the reported orthorhombic packing [12–14]. The two high angle peaks were not anticipated for Phase II, but they are precedented [41, 43]. Pure hexagonal packing is approached as the temperature is increased from 26 to 38°C (and the rate of rotation about the molecular long axes is increased consequently) since the high angle peaks move toward coalescence.

Table 3. Median temperatures ($\langle T \rangle$) and entropies (ΔS) of reversible transitions. Positive entropies are reported since calculations are based upon ΔH_h.

Compound	$\langle T \rangle$ /°C	ΔS/J g^{-1} K^{-1}
BS	10.8	0.026
	14.3	0.017
	25.9	0.36
1a	20.0	0.29
1b	14.5	0.59[a]
1c	19.7	0.64
1e	12.9	0.0080
	20.0	0.36
1f	3.7	0.038
	11.6	0.014
	24.0	0.35
C21	32.5	0.17[b]
	40.2	0.51[b]

[a] Transition not completely reversible; see text.
[b] From data in [12].

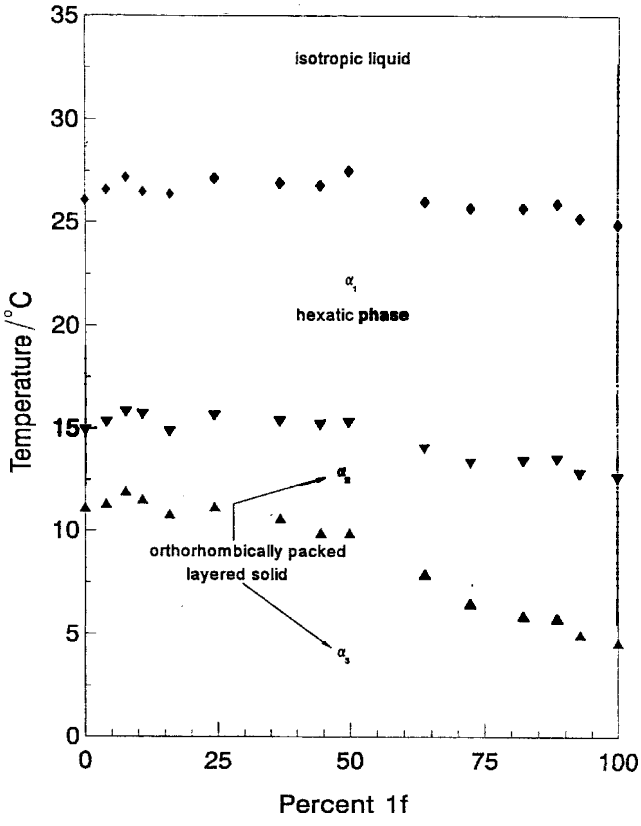

Figure 4. Phase transition temperatures of **BS/1f** mixtures as observed by DSC and plotted as a function of solvent composition.

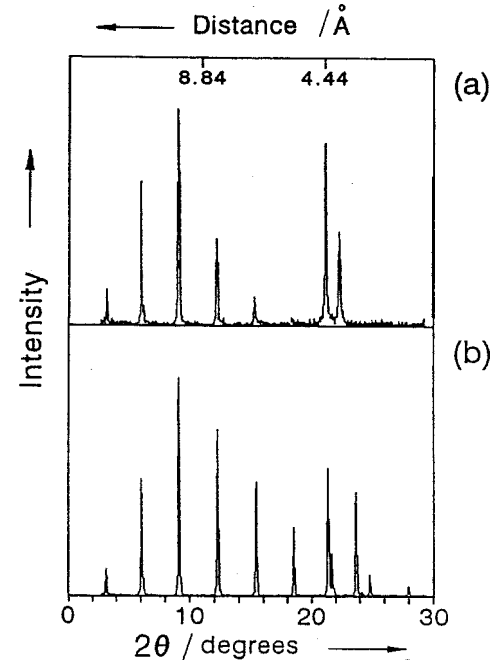

Figure 5. XRD patterns of **C21** at (*a*) 38°C and (*b*) 28°C.

In the α_3 phase of **BS**, figure 6(*a*), one high angle peak, corresponding to an intermolecular interlayer distance of 4.76 Å, is observed. Both Dryden [30] and Krishnamurti *et al.* [31] report a corresponding value of 4.73 Å. Five orders of the (0 0 0 1) spacing, corresponding to $d = 31.4$ Å, are observed. Two side spacings (4.28 and 3.89 Å) corresponding to intermolecular distances of 4.65 and 5.12 Å are calculated in the α_2 phase, figure 6(*b*); the previously reported values are 4.50–4.61 and 5.09–5.10 Å [30, 31]. The low angle portion of the α_2 diffractogram has essentially the same features ($d = 31.5$ Å) as the α_1, but they are indexed as (0 0 1). In the α_1 phase figure 6(*c*), the diffractions correspond to 4.21, 3.98, and 3.76 Å; Dryden reported two distances, 4.28 and 3.76 Å [30]. From the (at least) four orders of the (0 0 1) spacing, some long range packing order is seen to be present and $d = 31.2$ Å.

Diffraction patterns recorded at 15, 5, and −5°C (during cooling) and at 8 and 17.5°C (during warming), figure 7, indicate that **1a** forms a layered crystalline phase and a hexatic (probably SmB) phase whose layer thickness is 32.7 Å; the diffraction pattern at 15°C, figure 7(*b*) or 17.5°C is typical of a layered hexatic (α_1) phase with long range order—as indicated by a (0 0 0 3) reflection. Assuming that the $2\theta = 5.99°$ peak at 8°C is from the (0 0 2) reflection, the solid is layered, also. At 5°C, the presence of a small peak at 8.11° and a slightly broader (1 0 0) reflection suggest the continued presence of some α_1-like phase, probably as a result of hysteresis.

Small (< 5%) peak intensity differences were observed among diffractograms of **1b** (figure 8) obtained upon

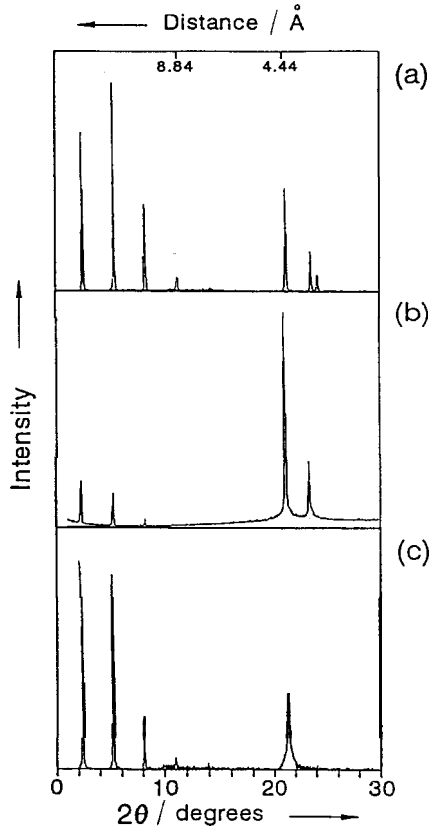

Figure 6. XRD patterns of **BS** at (*a*) 5°C, (*b*) 13°C, and (*c*) 18°C.

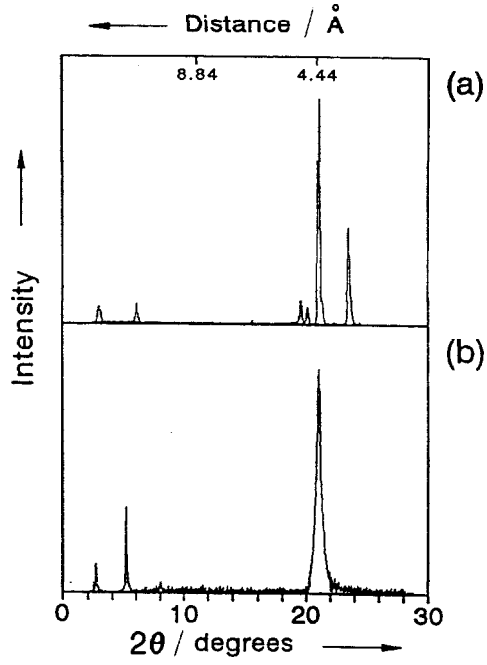

Figure 7. XRD patterns of **1a** at (*a*) 8°C (heating) and (*b*) 15°C (cooling).

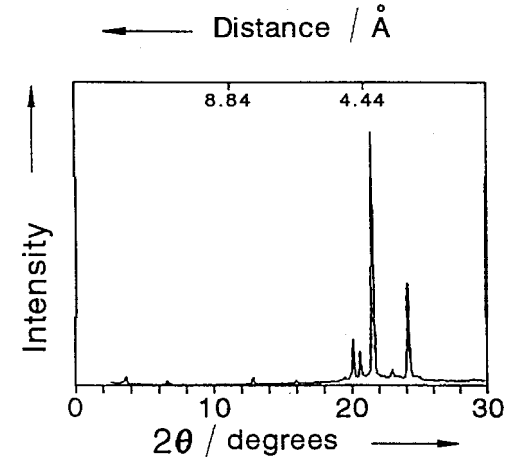

Figure 8. XRD pattern of **1b** at − 15°C.

cooling to − 15°C and heating to 10°C. Attempts to record the diffraction pattern of the narrow monotropic phase by cooling to 10°C from the isotropic phase were unsuccessful. We suspect that imprecise control of sample temperature, a small temperature gradient through the sample depth, and/or isothermal conversion to the thermodynamically more stable solid are responsible. The narrowness of the peaks at high angle and what appear to be (0 0 1), (0 0 2), and (0 0 4) reflections are consistent with a crystalline phase whose layer thickness (from the (0 0 4) reflection) is 27.9 Å.

Diffraction patterns of **1c** (figure 9) indicate a single anisotropic phase that is crystalline and possibly layered ($d = 28.0$ Å), but not hexagonally packed.

No hysteresis was detected by X-ray diffraction of **1d** (figure 10) during cooling or warming. At 5 and 12°C, a solid, layered phase ($d = 28.7$ Å) is present. At 14.4°C, two phases may be present: a layered crystal (N.B., (0 0 1), (0 0 2), and (0 0 3) low angle peaks) whose (1 0 0) high angle peak is very intense and somewhat broader

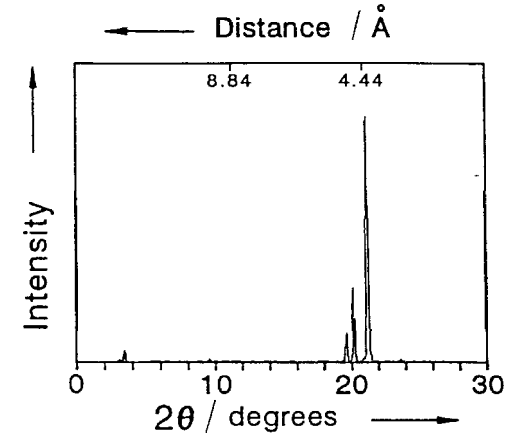

Figure 9. XRD pattern of **1c** at 10°C.

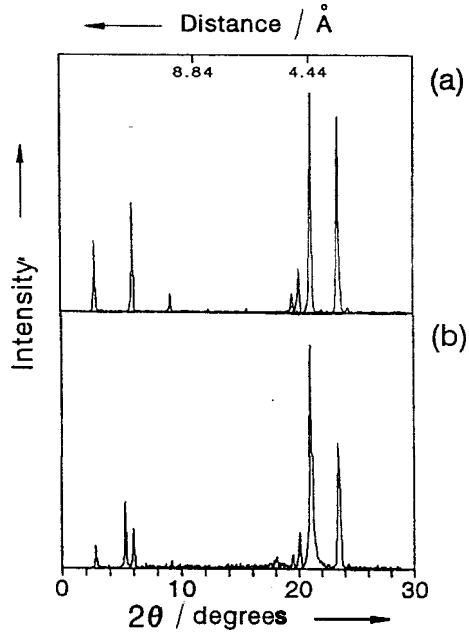

Figure 10. XRD patterns of **1d** at (*a*) 10°C and (*b*) 14.4°C.

than at lower temperatures; and a more disordered, possibly liquid crystalline phase of undetermined packing that is stable over a very narrow temperature range (N.B., the peaks at $2\theta = 19$–$21.5°$ resemble those of **1c**).

The high angle reflections of **1e** (figure 11) are consistent with a layered, crystalline phase at 5°C, figure 11 (*a*), and a smectic-like phase at 16°C, figure 11 (*b*). The 3.6 Å difference between the *d*-values of the two phases

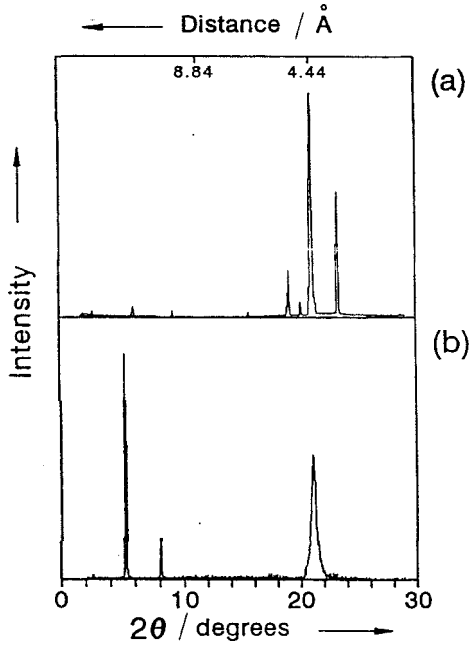

Figure 11. XRD patterns of **1e** at (*a*) 5°C and (*b*) 16°C.

(*c*. 28.8 Å at 5°C and 32.4 Å at 16°C) is the largest found in the set of isomeric esters.

Diffraction patterns of **1f** (figure 12) and **BS** are very similar, as expected from the miscibility studies. Although the values of *d* for **1f** are smaller than those of **BS** by as much as 0.8 Å, the differences lie within the sum of our experimental errors. Unexpectedly, the intensity of the (0 0 1) (or (0 0 0 1)) peak was lower than that of the (0 0 2) (or (0 0 0 2)) peak. Dipolar alignment of neighbouring molecules (producing a structure which has the dimensions of 1/2 unit cell (1/2*d*) within a layer and causing destructive interference of the (0 0 1) reflection) or the concave sample surface may be responsible.

Molecular packing within analogous **1f** and **BS** phases is quite similar except for the presence of a shoulder on the peak at $2\theta = 23.3°$ in the α_2 phase of **1f**. Either rotations of **1f** molecules about their long axes are too slow to average anisotropies [41, 43] or the sample was not fully temperature-equilibrated by our annealing procedure (see §5). In the α_1 phase of **1f**, the calculated intermolecular/intralayer distances are 4.74 Å.

At least three low angle reflections, not including (0 0 1), are present for **BS/1f** mixtures at 5°C, figure 13 (A). The presence of the (0 0 4) peak in all diffraction patterns demonstrates that long range order of the pure components is retained in the mixtures. There are two reflections at $2\theta > 20°$, suggesting α_2-type packing. However, lateral

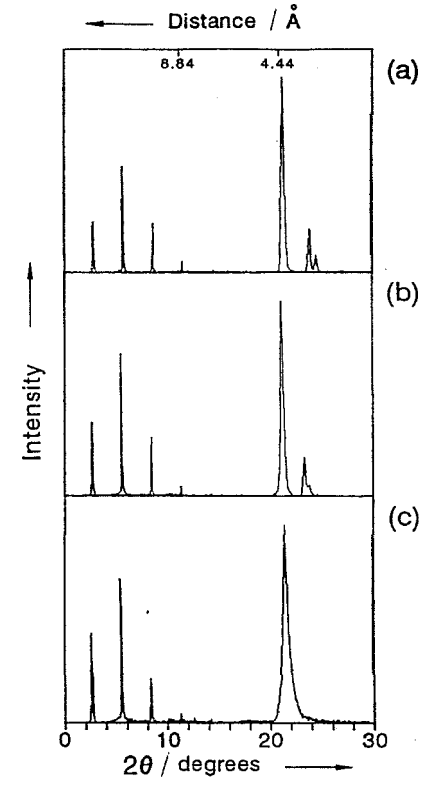

Figure 12. XRD patterns of **1f** at (*a*) 1°C, (*b*) 9°C, and (*c*) 18°C.

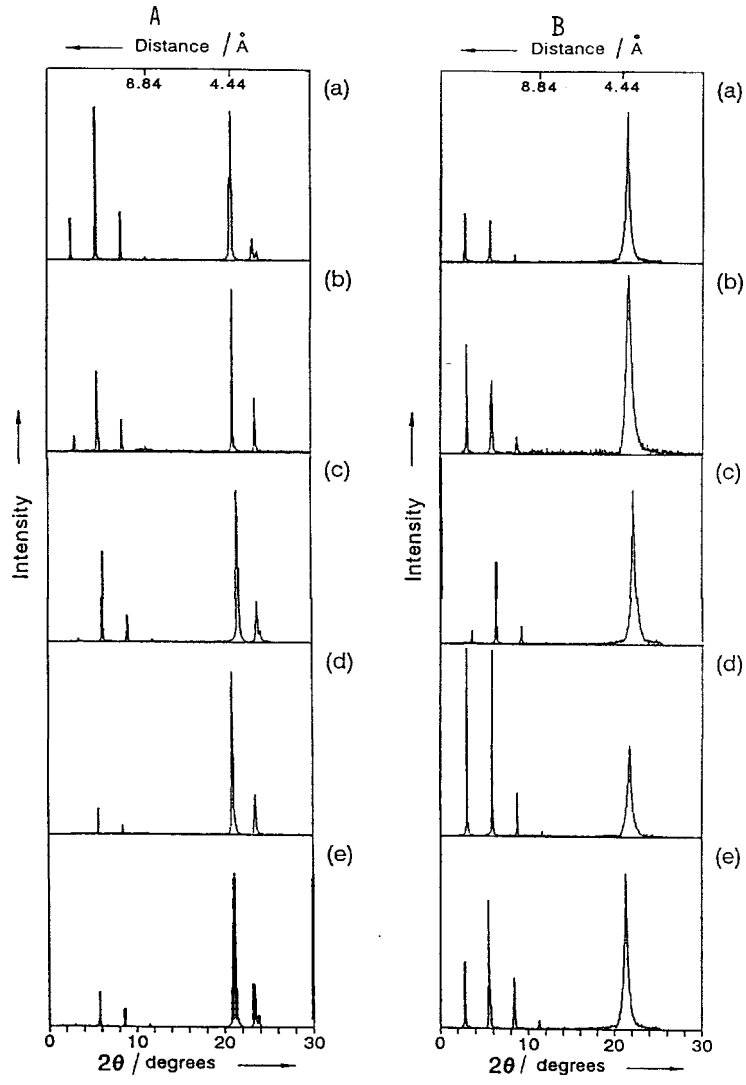

Figure 13. XRD patterns of **BS**/**1f** mixtures. Weight % of **1f** are (*a*) 0, (*b*) 25, (*c*) 50, (*d*) 75, and (*e*) 100: (A) at 5°C, (B) at 18°C.

rotational motion in the pure **BS** and **1f** phases is slower than in mixtures; neighbouring molecules interact more strongly in their neat phases. Mixtures at 18°C, figure 13(B), have the same packing arrangements and layer thicknesses. The (0 0 1) peak maxima in the mixtures are at $2\theta = 2.77$–$2.94°$ (i.e. $d = 31.9$–30.1 Å). By calculating the layer thickness from the (0 0 3) (or (0 0 4), when available) peak, precision and reproducibility are improved. The peak which appears at higher angle ($h\ k\ l = (1\ 1\ 0)$ and (2 0 0) superimposed) in each sample is at $2\theta = 21.57$–$21.71°$, corresponding to $D = 4.12$–4.09 Å (or intermolecular/intralayer distances in hexagonal arrays of the mesophases between 4.75 and 4.72 Å).

2.5. *Force field calculations of molecular lengths*

Utilizing the PCMODEL MMX force field [44], the same van der Waals molecular length, 32.0 Å, was calculated for all of the esters in their extended conformations. Although the default force field parameters employed are not optimized for alkyl alkanoates, the absolute error in the minimized geometries should not be large [44], and the relative errors should be even smaller. Given the very small differences between the MMX and X-ray derived *d*-values (table 4), all of the **1** molecules must, like the **BS**, be extended and lie orthogonal (or nearly so) to the molecular planes of their layers.

Table 4. Layer thicknesses, *d*, (Å) from XRD data and calculated extended molecular lengths, *l*, (Å) for **1f** and **BS**.

Compound		Phase α_1	Phase α_2	Phase α_3
BS	*d*	31.2 ± 0.3	31.5 ± 0.3	31.4 ± 0.2
	l	(32.0 Å)		
1f	*d*	30.8 ± 0.5	30.7 ± 0.4	31.0 ± 0.2
	l	(32.0)		

3. Discussion

3.1. *Factors influencing layered phases of simple, rod-like molecules: from alkanes to esters*

Although the simplest rod-like molecules, *n*-alkanes, form a variety of solid phases, none has been identified as a liquid crystal [12–14]. We take **C21** as a hydrocarbon model for **BS** and the positional isomers of **1** since all have a total of 19 linearly connected CH_2 units capped by methyl groups. Some longer *n*-alkanes have additional solid phases, but all of them are layered [12]. **C21** has two layered phases [45, 46]: in the lower temperature Phase I, chains are in all-*trans* conformations on average and are packed parallel to each other in an orthorhombic unit cell with very hindered rotation about the molecular long axis [45, 46]; in the higher temperature Phase II, molecules are still extended, but they are hexagonally packed in layers and can rotate relatively easily about their long axes [45, 46]. In fact, the arrangements of molecules in Phase I and Phase II of **C21** and in the α_2 and α_1 phases of **BS** are *analogous* to those of smectic E and smectic B mesophases [47, 48], but their mobilities are very different.

Several factors must be considered when assessing the influence on layer packing of inserting a carbonyl or carboxy group into an *n*-alkane chain. Since the group volume and bond angle to neighbouring carbon atoms of a carbonyl group are only *c.* 15% and *c.* 4° larger, respectively, than those of a methylene group [49–52], the intrinsic shapes and sizes of *n*-alkanes and *n*-alkanones with the same number of carbon atoms are very similar. There is no evidence for solid–solid transitions like those of the alkanes or **BS** from calorimetric studies on a limited number of 2− and symmetrical *n*-alkanones with carbon chain lengths comparable to that of heneicosane [33, 53]. This may be a result of stronger van der Waals interactions among dipoles of neighbouring carbonyl groups that is not counterbalanced by the entropy increase from lower barriers for rotation about H_2C–C(=O) single bonds (*vide infra*): group dipoles of methylene, carbonyl, and carboxy (*s-trans* ester) groups are 0.35, 2.4, and 1.8 D, respectively [54]. Regardless, up to 15% of 2-eicosanone, 2-heneicosanone, or 11-heneicosanone can be added to **C21** without observing significant changes in thermograms of the latter [55]; the alkanones must be incorporated nearly isomorphously into the **C21** lattice.

Like those of long *n*-alkanes, solid phases of *n*-alkanones consist of layers with molecules in extended conformations and oriented perpendicular to the layer planes [33, 53, 56]. 2-Alkanones appear to pack in pseudo-bilayers, so that the carbonyl groups from molecules in adjacent layers are near each other [56, 57].

Based upon the barriers to bond rotations, insertion of carboxy instead of carbonyl along an alkyl chain should *lower* the probability of chain deformation in a layered assembly: the barriers in dimethyl ether (C–O), propane (C–C), and acetone (C–C) are 13.0, 14.0, and 4.2 kJ mol^{-1}, respectively [58]. The *s-trans* conformer of a carboxy unit permits molecules like **BS** and **1** to fit better into their lattices than does the *gauche*-like *s-cis* conformer. However, the group dipole of the *s-cis* is *c.* 2 D larger than that of the *s-trans* [54*b*] and, therefore, more capable of stabilizing specific intermolecular interactions through van der Waals forces.

3.2. *Anisotropic phases of n-alkyl alkanoates*

There is surprisingly limited information regarding the mesomorphic behaviour of *n*-alkyl alkanoates. No acyclic, saturated, unbranched alkyl esters are listed in the volumes of Landolt–Börnstein devoted to liquid crystals [59, 60], and only two, **BS** and methyl stearate (**MS**), are found in the compilation of mesomorphic molecules by Demus *et al.* [61, 62]; a third molecule, 2-(2-hydroxyethoxy)ethyl dodecanoate, is not strictly a member of the set.

Evidence for polymorphism and possible mesomorphic phases, but not for enantiotropic liquid crystallinity, has been found in studies on methyl stearate (**MS**), ethyl stearate (**ES**), and propyl stearate (**PS**) (i.e. molecules in which the length of the 'acid' part is maintained at 18 carbon atoms and the length of the 'alcohol' part is shorter than in **BS**) [31, 32, 34, 53]. Since only 5% of the non-mesomorphic molecule, methyl palmitate, is needed to induce mesomorphism in **MS** [31], a reported transition between α-like phases of the neat material at 22°C [63] is probably due to impurities. Krishnamurti *et al.* [31] reported that **ES**, **PS**, and **BS** form ordered α phases; **PS** exhibits a monotropic mesophase that was not characterized. More recent evidence suggests that the highest temperature ordered-phases of **BS** and **PS** are very ordered smectics [34]. We have found no other reports of *n*-alkyl alkanoates being mesogenic.

We hypothesize that somewhat enhanced rotation of an alkoxy group of moderate length in these carboxy-inserted alkanes (perhaps in combination with dipolar effects; *vide ante*) induces sufficient disorder within molecular layers to transform the more ordered crystals into condis or liquid crystals.

3.3. *Anisotropic neat phases of **BS** and its **1** isomers*

Our data from **BS** neat phases are consistent with that of previous investigations: there are three (layered) α phases; the one at highest temperatures is SmB in character.

The data indicate that the morphologies of the corresponding α phases of **BS** and **1f** are of the same type: **1f** and **BS** are completely miscible, and their mixtures have transition temperatures that are only slightly dependent

upon composition; optical micrographs of neat **BS** or **1f** and their mixtures are very similar; the range of lattice dimensions in the mixtures, ± 0.5 Å for layer thicknesses and ± 0.05 Å for intermolecular spacings, are not significant. Thus, addition of **BS** to **1f**, or **1f** to **BS**, causes very little disruption of the lattice structure and the α_1 phase of **1f** is also SmB.

Polymorphism is also evident for **1a**, **1b** (on cooling only), **1d** and **1e**. The highest temperature anisotropic phases of both **1a** and **1e** are assigned as SmB-like since their optical micrographs and X-ray diffraction patterns are very similar to those of **BS** and **1f**. The monotropic phase of **1b** is smectic or a soft layered solid also, based upon its optical micrograph and the ease with which it is deformed by pressure.

In the highest temperature anisotropic phase of **1d**, the broadness of the most intense reflection (at $2\theta = 21.17°$) and the presence of a low angle diffraction suggest that the lattice has a range of intermolecular distances and is smectic. The optical micrograph further defines the phase as SmB.

The solid phases of **1a**, **1d** and **1e** have markedly similar diffraction patterns, particularly in the high angle region where there are four reflections. If these phases are orthorhombic, the Miller indices of the reflections are (1 0 0), (0 1 0), (1 3 0) and (2 2 0). In a coordinate system with the smallest spacing for the (0 1 0) reflection, the other spacings increase from (1 0 0) and (2 2 0) to (1 3 0). There is limited correspondence between the high angle peaks of **1b** and **1c** and those of **1a**, **1d** and **1e**. However, the small peak of **1b** at $2\theta = 22.95°$ is inconsistent with this indexing, and the expected highest angle (0 1 0) peak of **1c** is either not present or of very low intensity.

The evidence from diffraction data for layering in the crystalline phases is stronger for **1a** and **1d** than for **1b**, **1c** and **1e**. However, all of the crystalline esters exhibit low angle reflections. Assuming they are layered, the thicknesses range from 27.4 to 31.4 Å. The thinnest layers, 27.4 and 29.4 Å (for **1b** and **1c**, respectively), are from molecules whose carboxy groups are closest to the chain centre.

Within a layer, the disorder caused by the *steric* effects of an inserted carboxy group may be more easily tolerated when it is near the ends of a molecular, but attractive dipole–dipole interactions among neighbouring carboxy groups probably make a larger contribution near a layer middle. It is known that methylene groups of **C21** near a layer boundary experience much greater disorder than groups near the centre [45]. Thus, figure 14 shows that the clearing temperature of **1c** is anomolously high according to the trends established by **BS**, **1a** and **1b** on one side, and by **1d**, **1e** and **1f** on the other. Additionally, the sum of the heats of transition

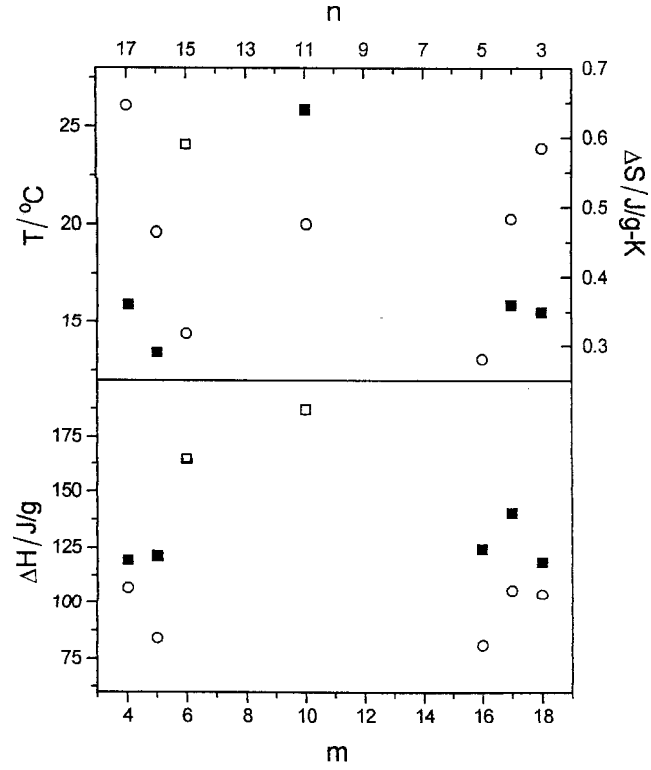

Figure 14. Temperatures (○) and entropies (■,) for clearing transitions (upper part) and the sums of the enthalpies (■,) and the enthalpies of clearing (○) for transitions on heating (lower part) versus m (the number of methylene units in the alkoxy part) and n (the number of methylene units in the alkanoate part) of **BS** and **1a**–**f**. The unfilled squares refer to the entropy change approximated for a monotropic phase (upper part) or the enthalpy changes of molecules that exhibit only one transition (lower part).

are highest for **1c** (with only *one* transition), *and* the enthalpy and entropy of the Phase II–isotropic transition of **C21** is smaller than the solid → isotropic transitions of **1b** and **1c** (tables 1–3) on a per gram basis. We suggest that analogous considerations apply here: in a layered phase, the carboxy groups of **1c** are forced to interact due to their proximity; in layers of the other isomers, efficient interactions among carboxy groups will occur if 50% lie near each layer boundary.

Unfortunately, it is not possible to determine with the information available the fraction of carboxy groups located near one layer boundary (except in the case of **1c**). Layered packing of conformationally-extended molecules with two carboxy groups equidistant from the chain ends, as in compounds **2** and **3** (i.e. diesters whose molecular lengths are near that of **BS**), requires that there be carboxy–carboxy group interactions among *all* neighbouring molecules. Such interactions appear to discourage efficient layer packing *or other arrangements leading to an ordered phase!* By DSC and POM, only one solid phase could be detected for **2** above -25°C

and **3** remained an isotropic liquid above − 25°C [64]. In addition, there is anecdotal evidence that the *direction* of the carboxy group with respect to a chain end may be a factor in phase formation. Whereas only a monotropic smectic-like phase was detected from **1b** (a hexyl ester), the smectic phase of **1d** (a hexanoate) is enantiotropic and exhibits a lower clearing temperature and a *much* lower enthalpy of transition.

$$\underset{\mathbf{2}}{\underset{\mathbf{3}}{H(CH_2)_mO(CO)(CH_2)_{12}(CO)O(CH_2)_mH}}\quad \begin{matrix} m \\ 2 \\ 4 \end{matrix}$$

Qualitative information concerning rotational motions of the esters can be obtained from comparisons of (1 0 0) or (1 0 0 0) peak shapes. For instance, the breadth of the (1 0 0 0) peak of **BS** in the SmB phase indicates a broad range of intermolecular spacings. Imperfections in the molecular lattice due to incomplete molecular extension or slight interdigitation, are probably transient. Also, pairs of molecules within a layer may prefer to adopt head-to-tail orientations (as suggested above), but diffusion within a layer will lead to temporal (and local) instabilities. From the XRD and DSC data, a model for the variations in molecular motions that accompany each phase change can be made. Since enthalpy changes for transitions between ordered phases of **BS** are small, their molecular packing is probably similar. A major differentiating factor is the rate of rotation of molecules about their molecular long axis. The decreased rates that accompany sample cooling lead to a collapse of the lattice into more dense arrays which retain essentially the same layer thickness. ^{1}H NMR line-width measurements, showing that intermolecular dipolar interactions increase between α_1 and α_3 [31–34], support this model [42].

4. Conclusions

The anisotropic phases of six structural isomers of **BS** have been characterized and compared both internally and with the solid phases of **C21**, the *n*-alkane from which they can be thought to derive. It is shown that the position of the carboxy group along the polymethylene chain is a very important factor in determining whether a smectic-like phase can be observed. Almost all of the anisotropic phases appear to be layered and either hexagonally or orthorhombically packed. The esters are excellent candidates for investigation of the basic factors that affect mesomorphism and for detailed exploration of the influence of an ordered host matrix on the reactivity of solute molecules [28, 65]. They complement the seminal studies of McBride and Hollingsworth on the modes of reaction of long-chained peroxyacid anhydrides in layered, crystalline phases [66].

5. Experimental

5.1. *Instrumentation*

NMR spectra were acquired on a Bruker AM-300 WB spectrometer with an Aspect 3000 computer. Infrared spectra were recorded on a Mattson Galaxy 5020 FT spectrometer (64 scans at 4 cm^{-1} resolution). Unless otherwise noted, all FTIR spectra are baseline corrected and were collected using a Specac ZnSe attenutated total reflectance (ATR) accessory with 45° crystal faces. Electron-impact mass spectra were obtained using the direct inlet probe of a Kratos MS-30 double focusing dual-beam spectrometer at 20 eV.

Melting points (corrected) and birefringent optical patterns were viewed at × 100 magnification from a Kofler hot-stage and a Bausch and Lomb microscope equipped with polarizing films. Temperature measurements were made using a calibrated thermistor. Photographs of birefringent patterns under crossed polarizers were obtained on an Olympus BH-2 microscope equipped with a home built hot stage and an Olympus C-35-AD-4 camera.

Analytical gas chromatography (GC) used a Perkin-Elmer 8500 or a Perkin-Elmer Autosystem chromatograph with flame ionization detectors. Both were equipped with a Hewlett-Packard HP-17 (50% phenyl and 50% methyl polysiloxane) 10 m × 0.53 mm fused silica capillary column.

Either a DuPont 910 or a Shimadzu DSC-50 differential scanning calorimeter (DSC) was employed for thermal analyses. The DuPont instrument was interfaced to a 1090B thermal analyser while the Shimadzu DSC was interfaced to a TA-501 thermal analyser and an IBM PC equipped with TA-50 version 2.2 thermal analysis software [67]. Heating curves were recorded followed by cooling curves. Samples of 5–10 mg were placed in uncrimped (to avoid leakage from capillary action) two-piece aluminum pans and scanned at 2°C min^{-1}. Calibration for heat change used an indium standard (Aldrich, 99.999%); the melting temperature of indium and the transition to the isotropic phase of **BS** were used for temperature calibration. All DSC curves were quantitatively reproduced during second heating–cooling cycles. A minimum of three and two runs have been averaged when error limits are or are not included, respectively.

Powder XRD patterns were collected on a Scintag 2000 X-ray powder diffractometer equipped with a liquid N_2 cooled solid state Ge detector and using CuK_α radiation (1.5406 Å). Data were analysed using a Digital Equipment Microvax 2000 computer. Samples (*c.* 400 mg) were placed in copper sample holders as liquids and allowed to solidify before placement on the sample stage. Prior to data collection (using a Lake Shore Cryotronics

temperature controller model DRC 91L, and a liquid N_2 bleed into the evacuated sample compartment), samples were thermally equilibrated for 10 min. Temperature was calibrated between 26°C and −20°C to an accuracy of ±0.5°C by warming and cooling standards (ethyl decanoate, Aldrich, 99+%, m.p. −20°C [68]; 1-decanol, Aldrich, 99+%, m.p. 7°C [67]; and **BS**, α_1–I, 26.1°C [31]) while following the intensity of their diffraction.

5.2. *Materials*

All esters with the exception of **BS** were synthesized in 59–98% yields according to standard acid chloride–alcohol coupling techniques [69] using commercially available acid chlorides and alcohols. A typical procedure for the synthesis of octadecyl butanoate (**1f**) is reported.

1-Octadecanol (Aldrich 99%) (27.0 g, 0.100 mol), was warmed to its liquid state and butanoyl chloride (Aldrich 98%) (17 ml, 0.150 mol), was added dropwise under a N_2 atmosphere during 15 min. The solution was heated under reflex for 30 min and then distilled under vacuum using a short path distillation apparatus. The purest fraction (according to GC analysis) was recrystallized repeatedly from acetone (Baker, 99.5%) to ⩾98% purity as determined by GC.

Pentyl heptadecanoate (***1a***). ^{1}H NMR ($CDCl_3$/TMS): δ 4.06 (2 H, t, J = 6.74 Hz, $-OCH_2-$), 2.29 (2 H, t, J = 7.41 Hz, $-C(O)CH_2-$), 1.62 (4 H, m, OCH_2CH_2- and $-C(O)CH_2CH_2-$), 1.26 (30 H, m, $CH_3(CH_2)_{15}-$), 0.89 (6 H, m, $-OCH_2CH_2CH_3$ and $CH_3(CH_2)_{15}-$). ^{13}C NMR ($CDCl_3$): 173.9 (C=O), 64.3 ($-OCH_2-$), 34.4 ($-C(O)CH_2-$), 31.9, 31.4, 29.7–28.9 (unresolved peaks), 28.7, 25.7, 25.0, 22.6, 22.5, 14.0 and 13.9 ppm. IR (neat): 2956, 2921, 2855, 1738, 1467, 1172 cm^{-1}.

Hexyl headecanoate (***1b***). ^{1}H NMR ($CDCl_3$/TMS): δ 4.06 (2 H, t, J = 6.80 Hz, $-OCH_2-$), 2.28 (2 H, t, J = 7.41 Hz, $-C(O)CH_2-$), 1.55 (4 H, m, $-OCH_2CH_2-$ and $-C(O)CH_2CH_2-$), 1.26 (30 H, m, $CH_3(CH_2)_{15}-$), 0.88 (6 H, m, $-OCH_2CH_2CH_3$ and $CH_3(CH_2)_{15}-$). ^{13}C NMR ($CDCl_3$): 173.8 (C=O), 64.3 ($-OCH_2-$), 34.4 ($-C(O)-CH_2-$), 31.9, 31.4, 29.6–29.0 (unresolved peaks), 28.6, 25.6, 25.0, 22.6, 22.5, 14.0 and 13.9 ppm. IR (neat): 2955, 2925, 2853, 1741, 1467, 1172 cm^{-1}.

Decyl dodecanoate (***1c***). ^{1}H NMR ($CDCl_3$/TMS): δ 4.05 (2 H, t, J = 7.03 Hz, $-OCH_2-$), 2.28 (2 H, t, J = 7.30 Hz, $-C(O)CH_2-$), 1.61 (4 H, m, $-OCH_2CH_2-$ and $-C(O)CH_2CH_2-$), 1.26 (30 H, m, $CH_3(CH_2)_{15}-$), 0.88 (6 H, m, $-OCH_2CH_2CH_3$ and $CH_3(CH_2)_{15}-$). ^{13}C NMR ($CDCl_3$): 173.8 (C=O), 64.3 ($-OCH_2-$), 34.4 ($-C(O)CH_2-$), 31.9, 29.6–29.3 (unresolved peaks), 29.2, 28.7, 25.9, 22.6, and 14.1 ppm. IR (neat): 2955, 2921, 2853, 1740, 1466, 1172 cm^{-1}.

Hexadecyl hexanoate (***1d***). ^{1}H NMR ($CDCl_3$/TMS): δ 4.07 (2 H, t, J = 6.80 Hz, $-OCH_2-$), 2.29 (2 H, t, J = 7.43 Hz, $-C(O)CH_2-$), 1.63 (4 H, m, $-OCH_2CH_2-$ and $-C(O)-CH_2CH_2-$), 1.27 (30 H, m, $CH_3(CH_2)_{15}-$), 0.91 (6 H, m, $-OCH_2CH_2CH_3$ and $CH_3(CH_2)_{15}-$). ^{13}C NMR ($CDCl_3$): 173.6 (C=O), 64.2 ($-OCH_2-$), 34.3 ($-C(O)CH_2-$), 31.9, 31.3, 29.6–29.6 (unresolved peaks), 29.4, 29.2, 28.7, 25.9, 24.6, 22.6, 1.0 and 13.8 ppm. IR (neat): 2956, 2932, 2853, 1741, 1467, 1171 cm^{-1}.

Heptadecyl pentanoate (***1e***). ^{1}H NMR ($CDCl_3$/TMS): δ 4.05 (2 H, t, J = 6.64 Hz, $-OCH_2-$), 2.29 (2 H, t, J = 7.30 Hz, $-C(O)CH_2-$), 1.61 (4 H, m, $-OCH_2CH_2-$ and $-C(O)CH_2CH_2-$), 1.26 (30 H, m, $CH_3(CH_2)_{15}-$), 0.91 (6 H, m, $-OCH_2CH_2CH_3$ and $CH_3(CH_2)_{15}-$). ^{13}C NMR ($CDCl_3$): 173.6 (C=O), 64.2 ($-OCH_2-$), 34.0 ($-C(O)CH_2-$), 31.9, 29.7–29.2 (unresolved peaks), 28.7, 27.0, 25.9, 22.6, 22.2, 14.0 and 13.6 ppm. IR (neat): 2957, 2919, 2861, 1744, 1467, 1173 cm^{-1}.

Octadecyl butanoate (***1f***). ^{1}H NMR ($CDCl_3$/TMS): δ 4.06 (2 H, t, J = 6.74 Hz, $-OCH_2-$), 2.28 (2 H, t, J = 7.46 Hz, $-C(O)-CH_2-$), 1.64 (4 H, m, $-OCH_2CH_2-$ and $-C(O)CH_2CH_2-$), 1.26 (30 H, m, $CH_3(CH_2)_{15}-$), 0.95 (3 H, t, J = 7.38 Hz, $-OCH_2CH_2CH_3$), 0.90 (3 H, t, J = 6.74 Hz, $CH_3(CH_2)_{15}-$). ^{13}C NMR ($CDCl_3$): 173.7 (C=O), 64.4 ($-OCH_2-$), 36.3 ($-C(O)CH_2-$), 32.0, 29.7–28.7 (unresolved peaks), 25.9, 22.7, 18.5, 14.1 and 13.7 ppm. IR (neat): 2955, 2927, 2854, 1741, 1467, 1179 cm^{-1}.

Synthesis of n-butyl stearate (***BS***) [16]. Boron trifluoride etherate (Aldrich, purified, redistilled) (100 ml, 0.813 mol), was cannulated under N_2 pressure into a N_2-filled flask containing 50.0 g (0.176 mol) of stearic acid (Aldrich 99+%) in 400 ml of previously distilled *n*-butanol (Baker, reagent, b.p. 114–115°C). The mixture was heated under reflux under N_2 for 4 h, cooled to room temperature, and 500 ml of anhydrous ether (Baker, 99.0%) added. The mixture was extracted with distilled water (2 × 200 ml), 20% w/v aqueous sodium bicarbonate (2 × 200 ml), distilled water (2 × 200 ml), and aqueous saturated sodium chloride (2 × 200 ml), and then dried over anhydrous magnesium sulphate. After evaporation *in vacuo* on a rotary evaporator, 60.6 g of a colourless oil was collected. It was irradiated through a Pyrex filter for 40 h using a 450 W Hanovia medium pressure Hg lamp and passed through an alumina (top)/silica (bottom) column around which heating tape (≈80°C) was wrapped. The resulting oil was distilled under vacuum (b.p. 174°C/0.07 mm Hg) to yield 46.2 g (77%) of a colourless oil that was free of both stearic acid and *n*-butanol by GC analyses. The phase transition temperatures, determined from DSC heating thermograms, are: α_3–α_2, 11.0°C; α_2–α_1, 14.7°C; α_1–I, 26.0°C (lit. 11.1, 14.8 and 26.1°C [13, 31]).

n-Heneicosane (***C21***) (Humphrey; > 99% by GC), was purified by Dr. Alberto Nuñez.

We are grateful to Prof. Robert Catchings of Howard University for the use of his powder diffractometer and to Mr. Michael Dean for recording the mass spectra. The National Science Foundation is thanked for its financial support of this research.

References

[1] Vertogen, G., and De Jeu, W. H., 1987, *Thermotropic Liquid Crystals. Fundamentals* (Berlin: Springer-Verlag).

[2] Curran, S. A., and Asrar, J., 1987, *Mol. Cryst. liq. Cryst.*, **148,** 255.

[3] Wunderlich, B., and Grebowicz, J., 1984, *Liquid Crystal Polymers II/III*, edited by N. A. Plate (Berlin: Springer-Verlag), p. 1.

[4] Kelker, H., and Hatz, R., 1980, *Handbook of Liquid Crystals* (Weinheim: Verlag Chemie), p. 2.

[5] Gray, G. W., and Winsor, P. A. (editors), 1974, *Liquid Crystals and Plastic Crystals*, Vol. 1 (Chichester: Ellis Horwood).

[6] Gray, G. W., 1962, *Molecular Structure and the Properties of Liquid Crystals* (London: Academic Press).

[7] Demus, D., 1990, *Liquid Crystals. Applications and Uses*, Vol. 1, edited by B. Bahadur (Singapore: World Scientific), p. 1.

[8] Demus, D., Diele, S., Grande, S., and Sackmann, H., 1983, *Advances in Liquid Crystals*, Vol. 6, edited by G. H. Brown (New York: Academic Press), p. 1

[9] See for instance Wunderlich, B., and Chen, W., 1996, *Liquid Crystalline Polymer Systems. Technological Advances*, edited by A. I. Isayev, T. Kyu, and S. Z. D. Cheng (Washington: American Chemical Society), Chap. 15.

[10] Weiss, R. G., 1998, *Polymer Liquid Crystals. Thermophysical and Mechanical Properties*, Vol. 3, edited by W. Brostow (London: Chapman & Hall), Chap. 1.

[11] Sheikh-Ali, B. M., and Weiss, R. G., 1991, *Liq. Cryst.*, **10,** 575; Sheikh-Ali, B. M., and Weiss, R. G., 1994, *Liq. Cryst.*, **17,** 605.

[12] Broadhurst, M. G., 1962, *J. Res. NBS*, **66A,** 241.

[13] Schaerer, A. A., Busso, C. J., Smith, A. E., and Skinner, L. B., 1955, *J. Am. chem. Soc.*, **77,** 2017.

[14] Ewen, B., Strobl, G. R., and Richter, D., 1980, *Faraday Soc. Discuss.*, **69,** 19.

[15] See for instance Jouti, B., Provost, E., Petitjean, D., Bouroukba, M., and Dirand, M., 1996, *J. mol. Struct.*, **382,** 49 and references therein.

[16] Nerbonne, J. M., and Weiss, R. G., 1979, *J. Am. chem. Soc.*, **101,** 402.

[17] Otruba, J. P. III, and Weiss, R. G., 1982, *Mol. Cryst. liq. Cryst.*, **80,** 165.

[18] Otruba, J. P. III, and Weiss, R. G., 1983, *J. org. Chem.*, **48,** 3448.

[19] Hrovat, D. A., Liu, J. H., Turro, N. J., and Weiss, R. G., 1984, *J. Am. chem. Soc.*, **106,** 5291.

[20] Hrovat, D. A., Liu, J. H., Turro, N. J., and Weiss, R. G., 1984, *J. Am. chem. Soc.*, **104,** 7033.

[21] Ganapathy, S., Zimmermann, R. G., and Weiss, R. G., 1986, *J. org. Chem.*, **51,** 2529.

[22] He, Z., and Weiss, R. G., 1990, *J. Am. chem. Soc.*, **112,** 5535.

[23] Treanor, R. L., and Weiss, R. G., 1987, *Tetrahedron*, **43,** 1371.

[24] Deval, P., and Singh, A. K., 1988, *J. Photochem. Photobiol.*, **42A,** 329.

[25] Nagamatsu, T., Kawano, C., Orita, Y., and Kunieda, T., 1987, *Tetrahedron Lett.*, 3263.

[26] Kunieda, T., Takahashi, T., and Hirobe, M., 1983, *Tetrahedron Lett.*, 5107.

[27] Weiss, R. G., 1988, *Tetrahedron*, **44,** 3413.

[28] Weiss, R. G., Ramamurthy, V., and Hammond, G. S., 1993, *Acc. chem. Res.*, **26,** 530.

[29] Baldvins, J. E., Cui, C., and Weiss, R. G., 1996, *Photochem. Photobiol.*, **63,** 726.

[30] Dryden, J. S., 1957, *J. chem. Phys.*, **26,** 604.

[31] Krishnamurti, D., Kristmamurthy, K. S., and Shashidhar, R., 1969, *Mol. Cryst. liq. Cryst.*, **8,** 339.

[32] Krishnamurthy, K. S., and Krishnamurti, D., 1970, *Mol. Cryst. liq. Cryst.*, **6,** 407.

[33] Sullivan, P. K., 1974, *J. Res. NBS*, **78A,** 129.

[34] Krishnamurthy, K. S., 1986, *Mol. Cryst. liq. Cryst.*, **132,** 255.

[35] (*a*) Sackmann, H., 1989, *Liq. Cryst.*, **5,** 49; (*b*) Gray, G. W., and Goodby, J. W. G., 1984, *Smectic Liquid Crystals. Textures and Structures* (Glasgow: Leonard-Hill), Chap. 10.

[36] Moncton, D. E., and Pindak, R., 1979, *Phys. Rev. Lett.*, **43,** 701.

[37] Leadbetter, A. J., Mazid, M. A., Kelley, B. A., Goodby, J., and Gray, G. W., 1979, *Phys. Rev. Lett.*, **43,** 630.

[38] Gray, G. W., 1962, *Molecular Structure and the Properties of Liquid Crystals* (New York: Academic Press).

[39] Brown, G. H., and Shaw, W. G., 1957, *Chem. Rev.*, **57,** 1049.

[40] Porter, R. S., and Barrall, E. M. III, 1969, *Acc. chem. Res.*, **2,** 53.

[41] (*a*) Sands, D. E., 1969, *Introduction to Crystallography* (New York: Benjamin); (*b*) Doucet, J., Denicolo, I., and Craievich, A., 1981, *J. chem. Phys.*, **75,** 1523.

[42] De Vries, A., 1985, *Mol. Cryst. liq. Cryst.*, **131,** 131.

[43] Kelusky, E. C., Smith, I. C. P., Elliger, C. A., and Cameron, D. G., 1984, *J. Am. chem. Soc.*, **106,** 2267.

[44] *PCMODEL*©, 1992, Fifth Edn., Serena Software, Bloomington, IN, USA.

[45] Maroncelli, M., Strauss, H. L., and Snyder, R. G., 1984, *J. chem. Phys.*, **82,** 2811.

[46] Kelusky, E. C., Smith, I. C. P., Ellinger, C. A., and Cameron, D. G., 1984, *J. Am. chem. Soc.*, **106,** 2267.

[47] Gray, G. W., and Goodby, J. W. G., 1984, *Smectic Liquid Crystals. Textures and Structures* (Glasgow: Leonard-Hill), Chap. 4.

[48] Kutsumizu, S., Yamada, M., and Yano, S., 1994, *Liq. Cryst.*, **16,** 1109 and references therein.

[49] Herzberg, G., 1967, *Electronic Spectra of Polyatomic Molecules* (Princeton, NJ: Van Nostrand).

[50] Sutton, L. E. (editor), 1965, *Tables of Interatomic Distances and Configurations in Molecules and Ions* (London: The Chemical Society).

[51] Sutton, L. E. (editor), 1958, *Tables of Interatomic Distances, Special Publication No. 11* (London: The Chemical Society).

[52] Kitaigorodsky, A. I., 1973, *Molecular Crystals and Molecules* (New York: Academic Press), p. 21.

[53] Vilalta, P. M., Hammond, G. S., and Weiss, R. G., 1993, *Langmuir*, **9,** 1910.

[54] (*a*) SMYTH, C. P., 1937, *J. chem. Phys.*, **4,** 209; (*b*) EXNER, O., 1975, *Dipole Moments in Organic Chemistry* (Stuttgart: Georg Thieme Verlag), p. 77.
[55] NUÑEZ, A., HAMMOND, G. S., and WEISS, R. G., 1992, *J. Am. chem. Soc.*, **114,** 10 258.
[56] BAILEY, A. V., MITCHAM, D., and SKAU, E. L., 1970, *Chem. Eng. Data*, **15,** 542.
[57] SAVILLE, W. B., and SHEARER, G., 1925, *J. chem. Soc.*, **127,** 591.
[58] FERGUSON, L. N., 1975, *Organic Molecular Structure* (Boston: Willard Grant Press), Chap. 18.
[59] VILL, V., 1992–3, *Liquid Crystals*, Vol. 7, parts a–c, Landolt-Börnstein, Group IV, edited by J. Thiem (Berlin: Springer-Verlag).
[60] KAST, K., 1960, *Eigenschaften der Materie ihren Aggregatzuständen*, edited by K. Schäffer, and E. Lax (Berlin: Springer-Verlag), p. 266.
[61] DEMUS, D., DEMUS, H., and ZASCHKE, H., 1974, *Flüssige Kristalle in Tabellen* (Berlin: Deutscher Verlag für Grundstoffindustrie).
[62] DEMUS, D., and ZASCHKE, H., 1984, *Flüssige Kristalle in Tabellen II* (Berlin: Deutscher Verlag für Grundstoffindustrie).
[63] GRIFFIN, A. C., and BUCKLEY, N. W., 1978, *Mol. Cryst. liq. Cryst.*, **41,** 141.
[64] BALDVINS, J. E., 1996, PhD. thesis, Georgetown University, USA.
[65] WEISS, R. G., 1991, *Photochemistry in Organized and Constrained Media*, edited by V. Ramamurthy (New York: VCH Publishers), Chap. 14.
[66] See for instance (*a*) MCBRIDE, J. M., 1983, *Acc. chem. Res.*, **16,** 304; (*b*) FENG, X. W., and MCBRIDE, J. M., 1990, *J. Am. chem. Soc.*, **112,** 6151; (*c*) HOLLINGSWORTH, M. D., and MCBRIDE, J. M., 1990, *Adv. Photochem.*, **15,** 279.
[67] TA-50WSI Thermal Analysis System, Windows Edition©, 1993, Shimadzu Corp., Kyoto, Japan.
[68] LIDE, D. R. (editor), 1990, *Handbook of Chemistry and Physics*, 71st Edn (Boca Raton, FL: CRC Press).
[69] MARCH, J., 1977, *Advanced Organic Chemistry*, 2nd Edn. (New York: McGraw-Hill), p. 361.